J Polym Res (2013) 20:66
DOI 10.1007/s10965-012-0066-4

ORIGINAL PAPER

Characterization and preparation of poly(vinylidene fluoride) (PVDF) microporous membranes with interconnected bicontinuous structures via non-solvent induced phase separation (NIPS)

Ping-Yun Zhang · Hu Yang · Zhen-Liang Xu · Yong-Ming Wei · Jun-Lian Guo · Dong-Gen Chen

Received: 17 August 2012 / Accepted: 19 December 2012 / Published online: 16 January 2013

Abstract Poly(vinylidene fluoride) (PVDF) membranes possessing interconnected bicontinuous structures with superior mechanical properties and improved hydrophilicity were obtained from PVDF/*N*,*N*-dimethylacetamide (DMAc)/Tween 80/water systems via non-solvent induced phase separation (NIPS) with 60 °C and ambient temperature casting solution. Tween 80/H_2O mixtures were adopted as dopant; water/ethanol (50:50, mass ratio) and ethanol were chosen as coagulants. The effects of process parameters in terms of variations in dopant contents, casting solution temperatures, and coagulant compositions on the phase inversion process and performance of the resultant membranes were investigated. During the demixing process, water diffused from the interior of Tween 80 reverse micelles, resulting in an accelerated precipitation rate and surface segregation process of the polar head groups of Tween 80. The high temperature of the casting solution contributed to enhancing the diffusion rate of liquid–liquid demixing on crystallization. The coagulant compositions changed the liquid–liquid and solid–liquid demixing dynamics of the casting solutions. Ethanol coagulant contributed to crystallization of PVDF/DMAc/Tween 80/water systems prior to liquid–liquid demixing. This delayed demixing process favored the formation of porous foliage-type top structures with fibril or lath bicontinuous fine structure of membrane bulk, increasing flux, and significant hydrophilicity improvement. Casting solutions in water/ethanol coagulant exhibited a less delayed demixing process with both liquid–liquid demixing and crystallization, resulting in formation of fine structure in the form of strings or stripes and limited hydrophilicity improvement. The predominant typical α- and β-type crystallinity in PVDF was attributed to the existence of dopants, the high temperature of the casting solution, and water/ethanol coagulant. This was consistent with the superior mechanical properties of the corresponding PVDF membrane. The newly developed hydrophilic PVDF membranes with superior mechanical properties and low-fouling of bovine serum albumin (BSA) are anticipated to be suitable not only for wastewater treatment, but also for bioseparation.

Keywords Mixture additives · Coagulants · Bicontinuous structure · Mechanical properties

Introduction

In recent decades, PVDF has received lots of attention as a membrane preparation material owing to its outstanding properties such as excellent chemical resistance (tolerates various acids and alkalies), thermal stability, mechanical strength and flexibility, oxidation resistance and exceptional hydrolytic stability, compared to other commercialized polymeric materials. The functions of PVDF membranes are greatly influenced by their physical morphology and chemical composition. Optimized structures of PVDF in terms of membrane surface properties, structures, and mechanical properties are anticipated for various applications

Electronic supplementary material The online version of this article (doi:10.1007/s10965-012-0066-4) contains supplementary material, which is available to authorized users.

P.-Y. Zhang · H. Yang · Z.-L. Xu (✉) · Y.-M. Wei · J.-L. Guo · D.-G. Chen
State Key Laboratory of Chemical Engineering, Membrane Science and Engineering R&D Lab, Chemical Engineering Research Center, East China University of Science and Technology, 130 Meilong Road, Shanghai 200237, China
e-mail: chemxuzl@ecust.edu.cn

in areas of purification and separation. Precise modulation of high-performance membranes with high hydrophilicity, high selectivity and fluxes, excellent mechanical properties, low fouling tendency, and defect-free production could yield effective oil–aqueous suspension solution systems [1, 2].

Phase separation methods have been developed for the preparation of porous membranes, e.g., thermally induced phase separation (TIPS) and non-solvent induced phase separation (NIPS). In either case, phase separation takes place in the form of liquid–liquid demixing and/or polymer crystallization, depending on phase behavior and preparative parameters, to yield polymer-poor and polymer-rich phases. The traditional TIPS method generally requires a high polymer concentration, a diluent, and a high dissolving temperature above the melting temperature of the polymer [3]. NIPS is the main technique used in the fabrication of PVDF membranes. It is used to cast a polymer solution on a suitable support and then to immerse it in a non-solvent coagulant. Cellular or finger-like pores are often formed in liquid–liquid demixing, whereas interlinked crystalline particles prevail in solid–liquid (crystallization) demixing. However, PVDF membranes with massive cellular pores and/or macrovoids usually show poor mechanical properties and undesirable selectivity. In comparison, membranes with bicontinuous interconnected networks show a favorable permeation flux, selectivity, and mechanical strength. It is generally accepted that both spinodal decomposition (liquid–liquid demixing) and crystallization (solid–liquid demixing) can lead to the formation of bicontinuous pore structure [4]. However, because of the complexity of the membrane formation mechanism, which is controlled by both kinetic and thermodynamic factors, many efforts have been devoted to modulate bicontinuous morphology to meet specific requirements via the NIPS process. The key factors determining the membrane formation process via NIPS are the polymer dope formulation, type of solvent and additive, the amount of additive, preparation temperature, and the composition of the coagulant. Additives and the composition of the coagulant medium play important roles in tuning membrane morphology. Additives commonly used as performance improvement agents include water [5–7], surfactant [8], surface-modifying macromolecules [9, 10], and mixture additives [11, 12]. As for coagulants, water is a well-known harsh non-solvent, which has a high diffusive rate with many solvents; whereas soft non-solvents include methanol, ethanol, and 1-octanol [13–15].

In our previous study, PVDF membranes prepared by incorporating Tween 80/water mixtures as dopants showed improved filtration and mechanical properties in that Tween 80 reverse micelles confined the diffusive movement of water from the interior of the casting solution [16]. Tween 80 is a water-soluble non-ionic surfactant with a strong affinity for water. H_2O molecules will be solubilized by reverse micelles when water is added into an *N*,*N*-dimethylacetamide (DMAc)/Tween 80 mixing medium, and a water pool of polar head groups of Tween 80 reverse micelles is formed (Supporting Information Fig. S1). The hydrogen bonds formed between polar head groups and water improve the stability of the reverse micelle structure, and the interconnection between the hydrocarbon chains of the reverse micelles and hydrophobic polymers could improve the thermodynamic stability of the casting solution and reduce the aggregation of polymer (incipient precipitation) caused by the non-solvent (Supporting Information Fig. S2). However, the instantaneous demixing of PVDF/DMAc/Tween 80/H_2O casting solution in water coagulant favored the formation of a skin layer followed by full development of finger-like macrovoids in the sub-layer of membranes, which limited the further improvement of separation properties. A promising approach to obtaining better-performing membranes is by modulating the sequence and the extent of liquid–liquid and liquid–solid demixing (crystallization). As a soft non-solvent, ethanol is not only used as a coagulant to slow down the precipitation rate, but also to post-treat pristine membranes [11]. On the basis that the mass transfer rate of different ethanol concentrations as coagulants with DMAc was in the order (PVDF/water) > (PVDF/water/ethanol) > (PVDF/ethanol) [15], water/ethanol of 50:50 mass ratio (A) and ethanol (B) were chosen as coagulants. When the casting solution was immersed in those coagulants, water diffusing out from Tween 80 reverse micelles broke the equilibrium of the interaction between polar head groups of the surfactant and water and the interconnection between PVDF and hydrophobic chains of the surfactant. Considering the surface segregation of the amphiphilic component indicated by X-ray photoelectron spectroscopy (XPS) analysis [17, 18], it is speculated that the confined diffusion of water by reverse micelles favors the surface segregation of polar head groups (hydrophilic groups) of surfactant in the casting solution, which improved the hydrophilicity of PVDF. The possible surface segregation process of polar head groups of Tween 80 is illustrated in Fig. 1. The effect of casting solution temperatures was also investigated.

Experimental

Materials

PVDF (Solef® 6010) was purchased from Solvay Advanced Polymers, L.L.C. (Alpharetta GA, USA). DMAc and ethanol were purchased from Shanghai Sinopharm Chemical Reagent Co. Ltd. (China). Tween 80 (HLB value 15.0) was yellow and supplied by Jiangyin Huayuan Chemical Co. Ltd. (China). Bovine serum albumin (BSA) (MW 67 K) was purchased from Lianguan Biochemical Reagent Company of Shanghai. Deionized water was prepared by our own lab. All chemicals used were of analytical grade and were used as received without any further purification.

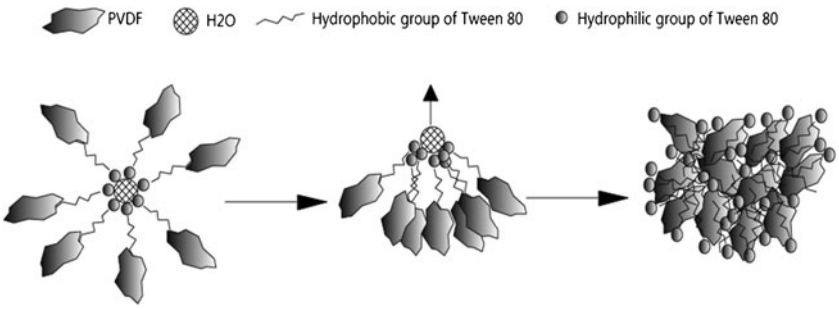

Fig. 1 Schematic of the surface segregation process of polar head groups of Tween 80 during demixing process

Measurements of casting solutions

Surface tension

The surface tension of the casting solution was measured by a JK99C automatic surface and interface tension measuring instrument (Shanghai Zhongcheng Digital Technology Apparatus Co. Ltd., China) via the Wilhelmy plate method at ambient temperature. Only the data at ambient temperature were measured because at high temperature the result may be inaccurate due to the volatility of DMAc and water.

Viscosity

The viscosities of PVDF casting solutions were obtained with a DV-II+ PRO digital viscometer (Brookfield, USA) at 298 K and 313 K, controlled by a water bath. The report data were taken at a shear rate of 50 s^{-1}.

Light transmittance

Light transmission experiments were used to mimic the precipitation kinetics of casting solutions in water/ethanol (A) and ethanol (B) coagulants. These experiments were carried out using a lab-made device as described by Zhang et al. [19]. A collimated laser was directed toward the glass plate immersed in the coagulants. The light intensity was captured by the detector and the data were recorded on a computer. The precipitation rate of the PVDF casting solution in the two coagulants could be characterized by curves of light transmittance versus immersion time.

Preparation of PVDF flat membranes

Different compositions of polymer dopants were prepared, after PVDF was completely dissolved at 60 °C, and the standing time of the casting solution was at least 12 hrs to eliminate internal bubbles. The homogeneous PVDF casting solutions were prepared both at 60 °C and at ambient temperature. The casting solutions were cast onto a glass plate at 25 °C and 60 % relative humidity by means of a glass rod, and then were immediately immersed in water/ethanol or ethanol coagulant (at 25 °C). The pristine membranes were kept in fresh water for 1 week, and the deionized water was changed thrice per day to ensure complete removal of residual solvent. Then the as-prepared membranes were kept in an ethanol bath until use. Pure PVDF membranes were white, whereas those membranes prepared using Tween 80/water as dopant went yellow. The preparation conditions of membranes are summarized in Table 1.

Membrane characterization

Filtration properties of resultant PVDF membranes

The filtration properties of the PVDF membranes were characterized by the determination of permeation flux (J), porosity (ε), and mean pore radius (γ_m). A round-shaped membrane with constant membrane area $A=2.289\times10^{-3}$ m^2

Table 1 PVDF membranes and the corresponding preparation conditions

Membrane	Dopant solution composition PVDF/DMAc/Tween 80/H_2O (wt%, mass ratio)	Coagulant composition Water/ethanol (wt%, mass ratio)	Temperature of casting solution (°C)
MH0T0W-A	18:82:0:0	50:50	60
MH3T0W-A	18:79:3:0		60
MH3T2W-A	18:77:3:2		60
MH3T3W-A	18:76:3:3		60
ML0T0W-A	18:82:0:0		RT
ML3T0W-A	18:79:3:0		RT
ML3T2W-A	18:77:3:2		RT
ML3T3W-A	18:76:3:3		RT
MH0T0W-B	18:82:0:0	0:100	60
MH3T0W-B	18:79:3:0		60
MH3T2W-B	18:77:3:2		60
MH3T3W-B	18:76:3:3		60
ML0T0W-B	18:82:0:0		RT
ML3T0W-B	18:79:3:0		RT
ML3T2W-B	18:77:3:2		RT
ML3T3W-B	18:76:3:3		RT

A coagulant composition, water/ethanol=50:50; *B* coagulant composition, water/ethanol=0:100; *RT* room temperature

was installed in a cell and the pressure in the cell was maintained at 0.1 MPa. Thus, pure water was forced to permeate through the membrane and the flux (J_w) was recorded. Then, 300 mg L^{-1} BSA was forced to permeate through the membrane at the same pressure and the flux (J_B) was recorded. To confirm the water flux recovery properties of these BSA-permeated membranes, the pure water flux (J_R) was measured after washing them with pure water three times for 0.5 h. The permeation flux (J) and flux recovery ratio (FRR) were calculated as follows [19, 20]:

$$J = \frac{V}{A \times t} \tag{1}$$

$$\mathrm{FRR}(\%) = \left(\frac{J_R}{J_W}\right) \times 100\% \tag{2}$$

where J is the membrane flux for pure water or BSA solution (L m^{-2} h^{-1}), V is the permeate volume of pure water or BSA solution (L), A is the membrane area, and t is the microfiltration time (h).

Porosity (ε) and mean pore size (γ_m) of the resultant membranes are defined by the following equation [16]:

$$\varepsilon = \frac{(m_1 - m_2)/\rho_G}{(m_1 - m_2)/\rho_G + \left(m_2 \middle/ \rho_p\right)} \times 100\% \tag{3}$$

where m_1 is the weight of the wet membrane (g), m_2 is the weight of the dry membrane (g), ρ_G is the density of ethanol (0.789 g cm^{-3}), and ρ_p is the density of the polymer (1.765 g cm^{-3}).

$$\gamma_m = \sqrt{\frac{(2.9 - 1.75\varepsilon) \times 8\eta l J_W}{\varepsilon \times A \times \Delta P}} \tag{4}$$

where η=8.9×10^{-4} Pa s (viscosity of pure water at 278 K), l is the thickness of the membranes, and ΔP is the operation pressure (0.1 MPa).

Dynamic contact angle (DCA) and elemental composition of top surface of PVDF membranes

A JC2000D1 (Shanghai Zhongcheng Digital Technology Apparatus Co. Ltd., China) system was used for the determination of dynamic contact angles (θ) of PVDF membranes at ambient temperature. A water droplet of 0.2 μL from a needle tip was dispersed on the membrane surface. The machine was coupled to a camera enabling image capture at 10 frames/s. Contact angles were determined from these images with the specific calculation software. In order to ensure that the results were sufficiently credible, experimental errors in measuring the θ values were evaluated to be less than ± 0.5°. Measurement for each set of samples was performed in triplicate and the average data of contact angles was taken.

The elemental composition of the top surface of PVDF membranes was determined using the energy dispersive X-ray spectroscopy (EDX) (Falcon, EDAX Inc., USA) feature of the electron microscope for elements which have a characteristic signal. The analysis indicated the existence and mass ratios of oxygen, fluorine, and carbon in the top surface of various membranes.

Morphology of PVDF membranes

The top-surface and cross-section morphologies of membranes prepared under various conditions were observed using scanning electron microscopy (SEM) (JEOL, JSM-5600LV). The samples were first immersed in liquid nitrogen, fractured, and then sputtered with gold.

Crystalline structures and mechanical properties of PVDF membranes

Measurements of mechanical properties were conducted by using a QJ210A instrument (Shanghai Qingji Instrument Technology Co. Ltd., China) at ambient temperature. The flat sample of settled width of 15 cm was clamped at both ends and pulled under tension at a constant elongation speed of 50 mm min^{-1} with an initial length of 25 cm. Break strength, elongation at break, and Young's modulus were obtained from the stress–strain curves through the average of at least five measurements.

The crystalline structures of the resultant membranes were investigated using X-ray diffraction (XRD) with a D/max-rB diffractometer (Rigaku, Japan) equipped with graphite monochromated Cu Kα radiation (λ=0.15405 nm) operated at 100 mA and 40 kV from 3 to 50°. Furthermore, the crystallinity of membranes was determined by a peak deconvolution method. The diffraction peaks at 2θ=18.2° and 20.4° were decomposed into amorphous and crystalline regions by Jade+ (MDI, Livermore, CA) analysis software. The crystallinity was defined as follows [21]:

$$\mathrm{Crystallinity}(\%) = \frac{A_c}{A_c + A_a} \times 100\% \tag{5}$$

where A_c is the area of the crystalline phase and A_a is the area of the amorphous phase. For all the samples, the area measurements were performed twice and averaged.

Results and discussion

Basic physicochemical properties of casting solutions

The basic physicochemical properties of the casting solutions are described in terms of surface tension, viscosity, and precipitation kinetics. Surface tension is related to the surface

arrangement of molecules at the interface between air and liquid. As shown in Fig. 2, the surface tension decreases as a result of the addition of Tween 80/H_2O dopants. The interaction between polar head groups of the surfactant and water provided a balanced resistance to the interconnection between PVDF and hydrophobic chains of the surfactant, which enhanced the thermodynamic stability of the casting solution [22]. At this point, it is noted that the surface of the casting solution is covered by the hydrocarbon chains of Tween 80, a feature which is related to the decreasing surface tension.

Figure 3 reveals an increasing viscosity of the casting solutions as Tween 80/H_2O dopant is added both at 60 °C and at ambient temperature. The casting solution at ambient temperature has higher viscosity. Increasing viscosity reveals a stronger interconnection between molecules [23]. The interconnection between polymer and reverse micelles enhanced the degree of chain entanglement of PVDF, which induces increasing viscosity (Supporting Information, Fig. S3). The lower viscosity of the casting solution at high temperature is attributed to less tight interconnections caused by the thermal movement of molecules [24, 25].

Precipitation kinetics of casting solutions by dynamic light transmittance

The dynamic demixing process of the casing solution in the two coagulants is illustrated in Fig. 4. The curves show delayed demixing in the two coagulants, especially in ethanol. A high concentration of dopant and a high temperature of the casting solution lead to a high precipitation rate. The order of precipitation rate of various casting solutions in the two coagulants is (H-A) > (L-A) > (H-B) > (L-B).

The reasons behind that behavior are as follows. Reverse micelles with a hydrocarbon chain shell of Tween 80 formed in the DMAc medium and these enhance the immiscibility

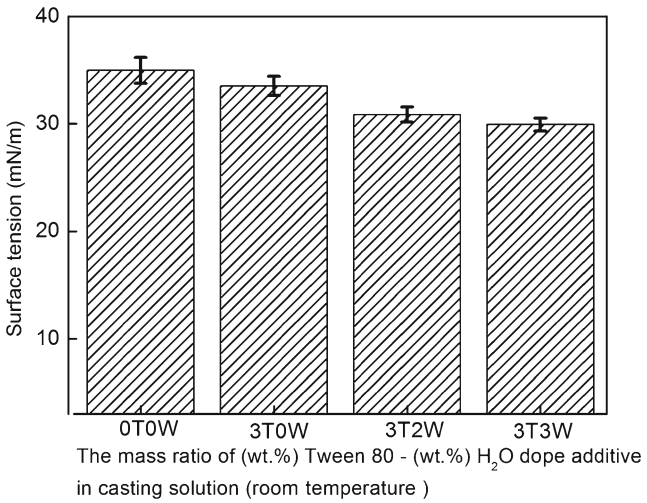

Fig. 2 Surface tension of casting solutions with different mass ratios of Tween 80/water dopant

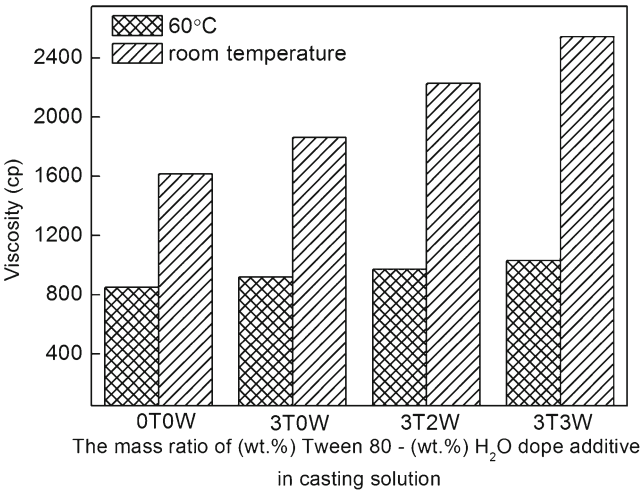

Fig. 3 Viscosities of casting solutions with different mass ratios of Tween 80/water dopants at 60 °C and room temperature (RT)

between casting solution and coagulants. This explains the accelerated demixing process in the presence of Tween 80. Moreover, further addition of water contributes to increasing immiscibility, and further enhances the precipitation rate of the casting solution [26]. Additionally, water diffusing out from the interior of the casting solution during the demixing process also accelerates this process. Heat transfer is thought to be faster than mass transfer, and a high temperature of the casting solution results in enhancing the diffusion rate of liquid–liquid demixing on crystallization; whereas the lower mass transfer rate between pure ethanol and DMAc explains the more delayed demixing process of casting solution in ethanol coagulant. Together with Fig. 3, which showed that viscosity increases after the addition of Tween 80/H_2O dopant, these results reveal that viscosity change is not the dominant factor in determining the precipitation rate.

Membrane performance

The resultant membranes are characterized by filtration properties in terms of J_W, J_B, and J_R as shown in Table 2. Compared with the maximum water flux of 192 L m^{-2} h^{-1} in membranes prepared from water coagulant, these results show that the delayed demixing process in water/ethanol and ethanol coagulants is favorable for flux improvement [16]. Table 2 shows that membranes prepared with ambient temperature casting solution have larger flux than those prepared at high temperature. Besides, it indicates that FRR improves after the addition of Tween 80/water dopants. J_W, J_B, and J_R decrease when Tween 80 is used as the sole additive and they sharply decrease with further addition of water. However, J_W, J_B, and J_R decrease and then increase with increasing concentration of dopants in the casting solution. The reasons for the downward and upward trends of J_W, J_B, and J_R in the presence of water are as follows. The accelerated precipitation rate of the casting

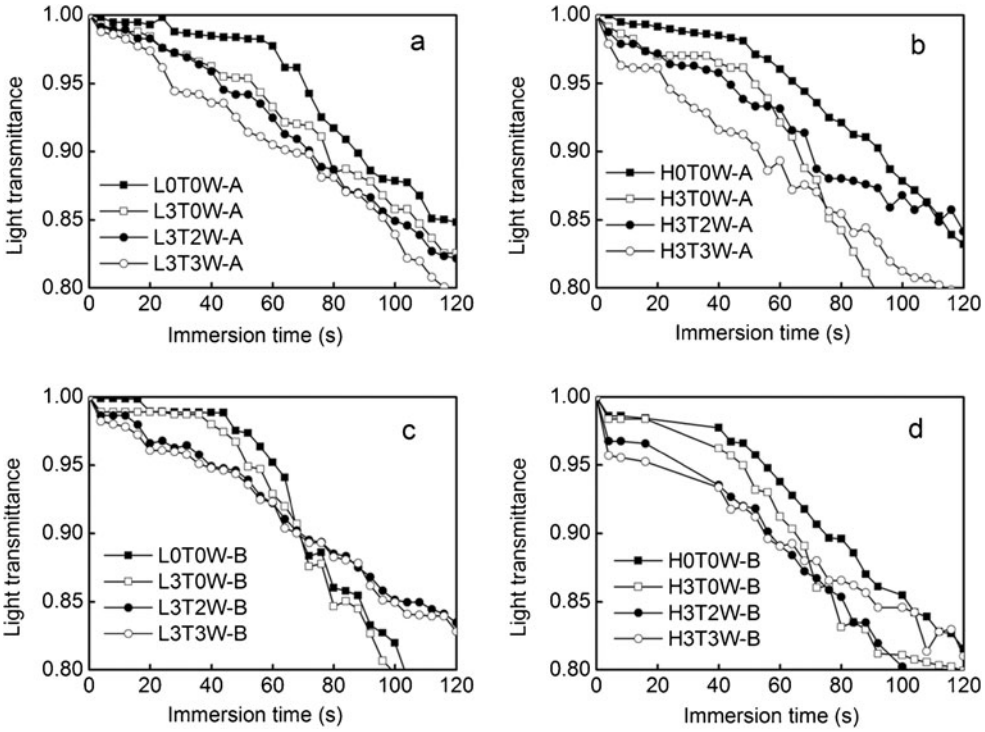

Fig. 4 Precipitation rates of different casing solutions under various preparation conditions

solution caused by the addition of water leads to decreasing J_W, J_B, and J_R at first, whereas, with increasing concentration of water, more water diffuses from the interior of the casting solution during the demixing process and works as a pore-forming additive. This is beneficial to the increase of J_W, J_B, and J_R. Moreover, Table 2 demonstrates that membranes prepared from ethanol coagulant at ambient temperature have higher flux and FRR. Comprehensive analysis of the various precipitation rates as shown in Fig. 4 suggests that the more delayed demixing process is beneficial to the formation of porous structures, which explains the increasing flux.

Because of the complex nature of the physicochemical interactions, the fine surface morphology (form and distribution) and the connected pores on DCA of PVDF membranes, it is not easy to interpret the membrane hydrophilicity only with DCA. However, it is possible to provide some information on the change of hydrophilicity of the resultant membranes caused by dopant contents, coagulant compositions, and casting solution temperatures. The DCA is characterized by curves of water drop angle versus contact time as shown in Fig. 5. The curves indicate that MH(L)0T0W-A(B) have excellent hydrophobic properties with large start contact angles (or advancing contact angle) and steady high receding contact angle θ_E (or equilibrium contact angle). However, the discrepancy in θs and θ_E of MH(L)-B containing Tween 80/H_2O dopant significantly increases with measurement time. The fast increase in the rate of reduction of the contact angle reveals an improvement in the hydrophilicity of the sample surface [17, 18]. Since membrane hydrophilicity has a pronounced effect on the BSA-fouling properties. The DCA

Table 2 Separation properties of PVDF membranes prepared under various conditions

Membrane	J_W (L m^{-2} h^{-1})		J_B (L m^{-2} h^{-1})		J_R (L m^{-2} h^{-1})		FRR (%)	
	A	B	A	B	A	B	A	B
MH0T0W	420±3.4	3,720±1.9	115±3.1	1,230±1.8	150±2.8	1,250±7.7	38.8±1.2	33.8±0.8
MH3T0W	210±4.2	3,360±7.3	190±9.8	990±5.1	210±2.2	1,700±7.2	50.1±0.6	50.7±1.1
MH3T2W	90±4.5	320±7.5	70±3.9	100±2.9	40±4.2	100±1.1	51.7±1.3	55.3±0.6
MH3T3W	270±3.4	1,670±3.3	120±2.1	470±9.6	160±7.8	1,070±1.6	61.4±0.8	64.0±0.8
ML0T0W	690±1.9	4,090±7.7	160±2.3	1,390±3.8	270±7.5	1,770±5.2	40.1±1.1	43.2±0.3
ML3T0W	610±4.3	3,650±3.6	160±2.4	990±1.3	270±6.6	1,700±2.9	45.0±0.3	46.7±1.3
ML3T2W	210±1.3	430±3.4	70±5.1	80±3.8	100±3.0	210±8.0	48.7±0.5	50.3±0.6
ML3T3W	480±3.2	1,800±2.1	130±4.7	650±7.7	280±1.5	1,220±4.2	59.1±1.7	56.3±0.7

A coagulant

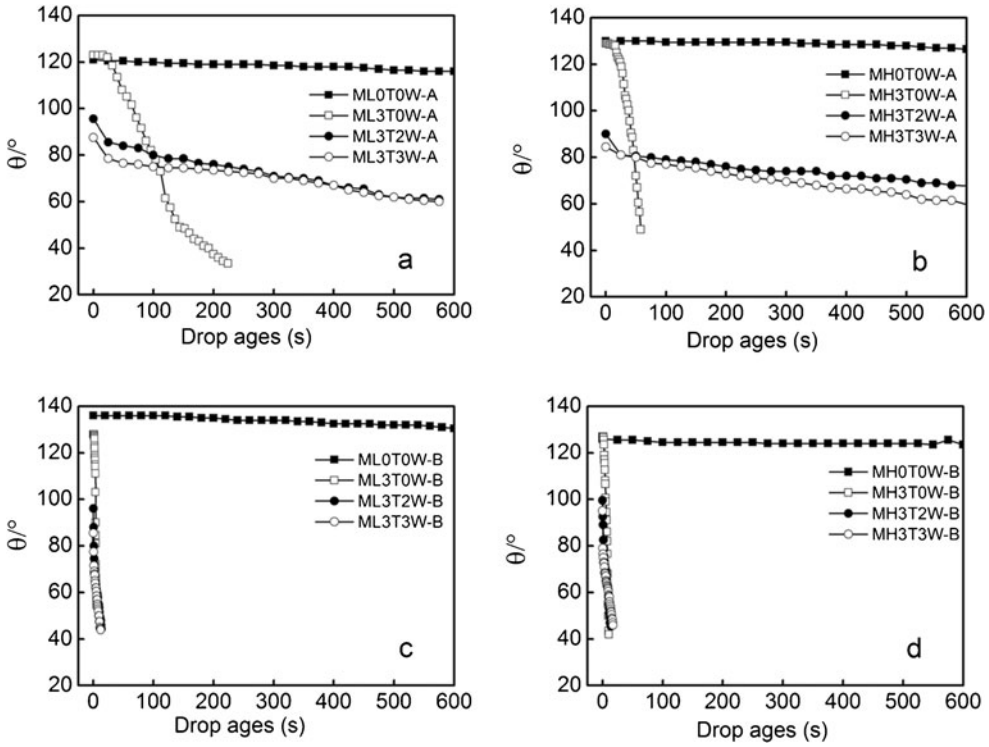

Fig. 5 Dynamic contact angles of PVDF membranes prepared under various conditions

results are consistent with the FRR improvement of the final membranes. Combining these results with the data on porosity and mean pore size of the resultant membranes as shown in Table 3, especially that of MH (L)3T2W-B, demonstrates that the contact angle of the resultant membranes does not originate in the porosity or mean pore size, but rather the surface segregation of polar head groups of Tween 80 during the demixing process [27].

The surface segregation of Tween 80 is further evidenced by EDX analysis as shown in Table 4. The results demonstrate that the content of oxygen in the top surface of the resultant membranes increases in the presence of Tween 80, and it further increases as water is added. The confined diffusion of water by reverse micelles favored the surface segregation of polar head groups of the surfactant in the casting solution, which improved the hydrophilicity of PVDF. With respect to the aforementioned physicochemical property of the casting solution, membranes prepared with the more delayed demixing process possess larger oxygen contents; whereas the less delayed demixing of PVDF/DMAc/Tween 80/water systems confines the surface segregation of Tween 80, which explains the limited hydrophilicity improvement of the resultant membranes.

Table 3 Porosities and mean pore size of membranes prepared under various conditions

Membrane	Mean pore size (nm)		Porosity (%)	
	A	B	A	B
MH0T0W	44	149	81.5±0.5	91.0±0.2
MH3T0W	29	121	78.9±0.7	89.5±0.1
MH3T2W	22	45	68.2±0.5	80.8±0.4
MH3T3W	32	100	79.4±0.7	85.9±0.7
ML0T0W	53	149	83.7±0.3	91.2±0.5
ML3T0W	59	147	82.0±0.1	90.0±0.5
ML3T2W	32	45	78.8±0.4	81.7±0.3
ML3T3W	40	105	81.9±0.7	86.8±0.7

A coagulant composition, water/ethanol=50:50; *B* coagulant composition, water/ethanol=0:100

Table 4 Elemental composition of the top surface of PVDF membranes

Membrane	O (%, mass ratio)	F (%, mass ratio)	C (%, mass ratio)
MH0T0W-A	4.27	49.41	46.32
MH3T0W-A	4.45	46.54	48.38
MH3T3W-A	4.59	48.33	47.21
ML0T0W-A	4.16	49.10	46.74
ML3T0W-A	4.33	48.35	47.33
ML3T3W-A	5.07	48.09	47.32
MH0T0W-B	3.89	48.78	47.33
MH3T0W-B	4.57	47.79	47.64
MH3T3W-B	5.11	47.35	47.54
ML0T0W-B	4.25	48.32	47.43
ML3T0W-B	5.20	45.91	48.85
ML3T3W-B	5.24	45.86	48.94

A coagulant composition, water/ethanol=50:50; B coagulant composition, water/ethanol=0:100

Membrane morphologies

The membrane morphologies were verified by SEM images of the top surface and cross section as shown in Figs. 6 and 7. All membranes reveal identifiable sponge-like cross-sectional structure with various morphologies of the top surface, which are significantly different from that of the asymmetric morphology of the skin layer with finger-like macrovoids prepared from water coagulant. Those changes in morphology are induced by the delayed demixing in coagulants containing ethanol.

Firstly, the top-surface morphologies of various membranes prepared with ambient temperature casting solutions were studied. Figure 6 reveals that the top surface of ML0T0W-A has the typical agglomerates of globules, which results in a loose arrangement [28]. The globule packing of ML3T0W-A is substantially denser than that of pure PVDF. On further addition of water, the globules are replaced by lotus-shape-type agglomerates with a dense packing arrangement, whereas membranes prepared from ethanol coagulant display significant differences. As a result of the more delayed demixing process, ML0T0W-B appears as a loose arrangement of elongated globules with sheet-type structures. The top surface of ML3T0W-B has wide stripe-shape solid entities. After further addition of water, the stripe-shape nanograins are further elongated and grouped in a foliage arrangement. Simultaneously, the foliage nanograins are clustered in agglomerates, appear to be attached to the structural entities that dominate the interior of the solid entities, and are well connected with others. Furthermore, as the concentration of water increases, the nanograins become slim and similar in size. A comparison of Figs. 6 and 7 shows that a high temperature of the casting solution is beneficial to the formation of larger sized agglomerates of nanograins with various configurations.

High magnification was then used to elucidate the interior cross section of the sponge-like membrane bulk. Figure 8 shows that such PVDF nanograins which construct the

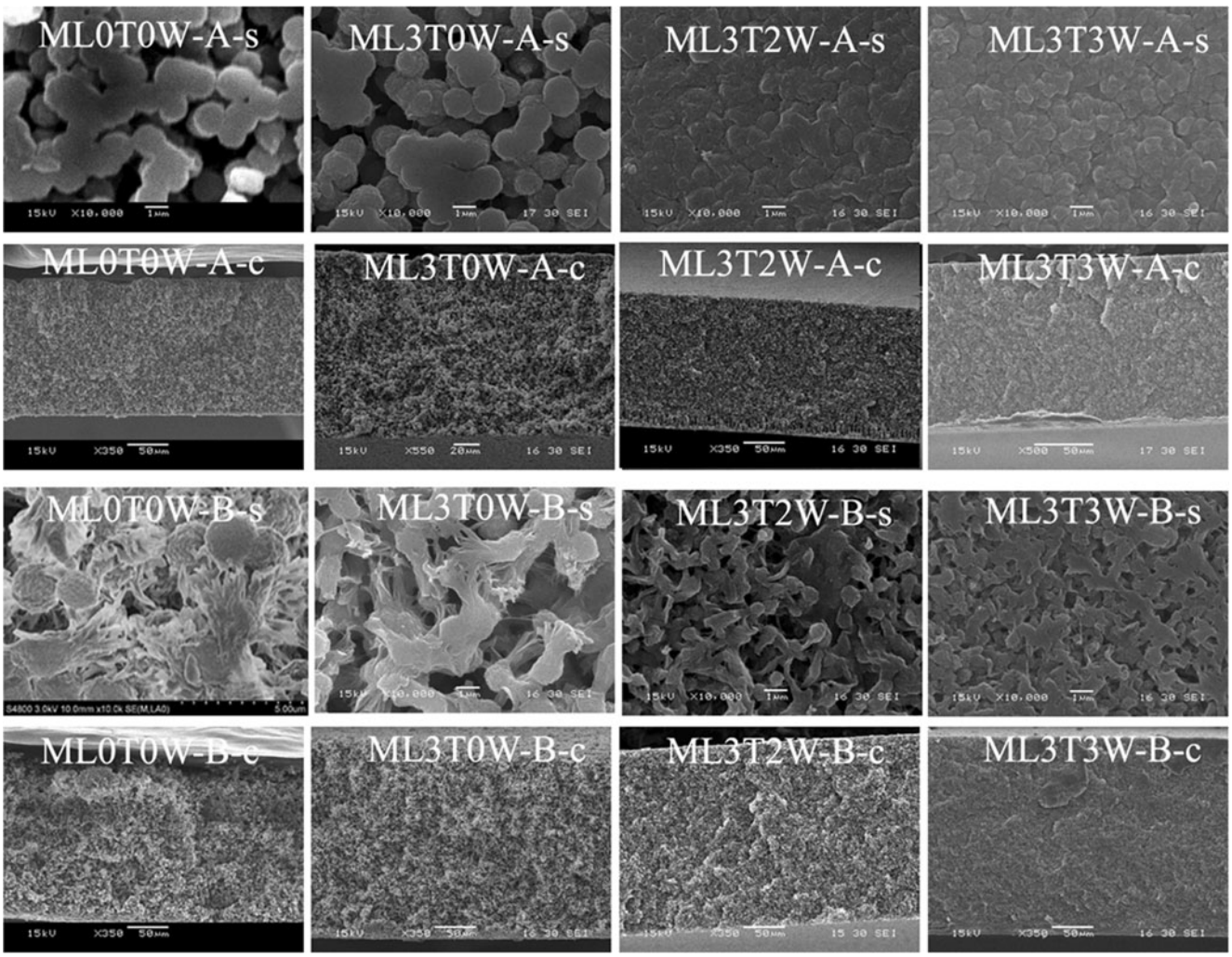

Fig. 6 SEM images of PVDF membranes prepared in two coagulants with room temperature casting solution (*s* top-surface structure, *c* cross-sectional structure)

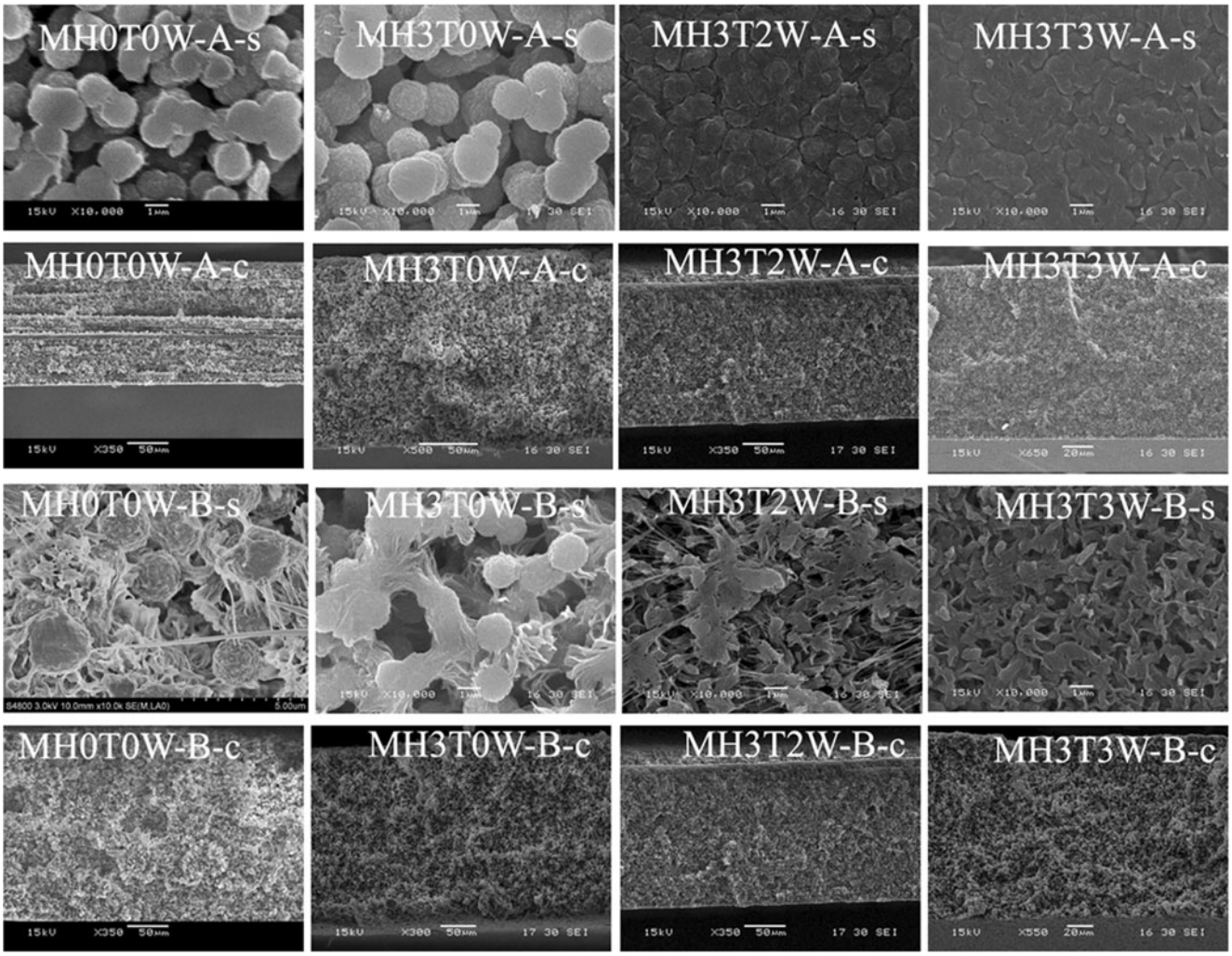

Fig. 7 SEM images of PVDF membranes prepared in two coagulants with 60 °C casting solution (*s* top-surface structure, *c* cross-sectional structure)

membrane bulk represent a crystallization-dominated phase separation, wherein all crystalline particles are nucleated and grown in a similar concentration field and finally fused together to form a bicontinuous structure [29]. The delayed demixing process in water/ethanol and ethanol coagulants determines the particulate bicontinuous configuration. A comparison of the membrane bulk of M(H)L0T0W-A(B) and M(H)L3T0W-A(B) confirms that the interconnection between polymer and surfactant is favorable for regular and close-packing of nanograins. A high temperature of the casting solution containing dopants in water/ethanol coagulant results in a less delayed demixing process, which explains the formation of agglomerates with increasing size. Still, the confined diffusion of water from Tween 80 reverse micelles during the demixing process makes the interaction between polar head groups of the surfactant and water provide unbalanced resistance to the interconnection between PVDF and the hydrophobic chains of the surfactant. This induces the further elongation of nanograins with similar size in the membrane bulk. In particular, M(H)L3T3W-A contains a bicontinuous fine structure in the form of strings or stripes, whereas M(H)L3T3W-B has fibril or lath bicontinuous fine structure. This reveals that the crystallization of membranes prepared from ethanol occurred prior to liquid–liquid demixing, which explains the change of string or stripe nanograins to foliage type.

Previous reports showed that the lotus-shape-type configuration of morphology is beneficial to a hydrophobic improvement [30]. However, in our current work the membrane with lotus-shape-type configuration shows that its hydrophilicity improves. Besides, together with the filtration properties discussed in Sect. "Membrane performance", it reveals that the contact angle of membranes does not originate in porosity. Nevertheless, it is believed that the polar head groups of Tween 80 are self-segregated on the top surface of the membranes, resulting in hydrophilicity improvement. Furthermore, the dense packing of the lotus-shape-type nanograins explains the decreasing flux, whereas the porous structures of bicontinuous foliage type increase the flux.

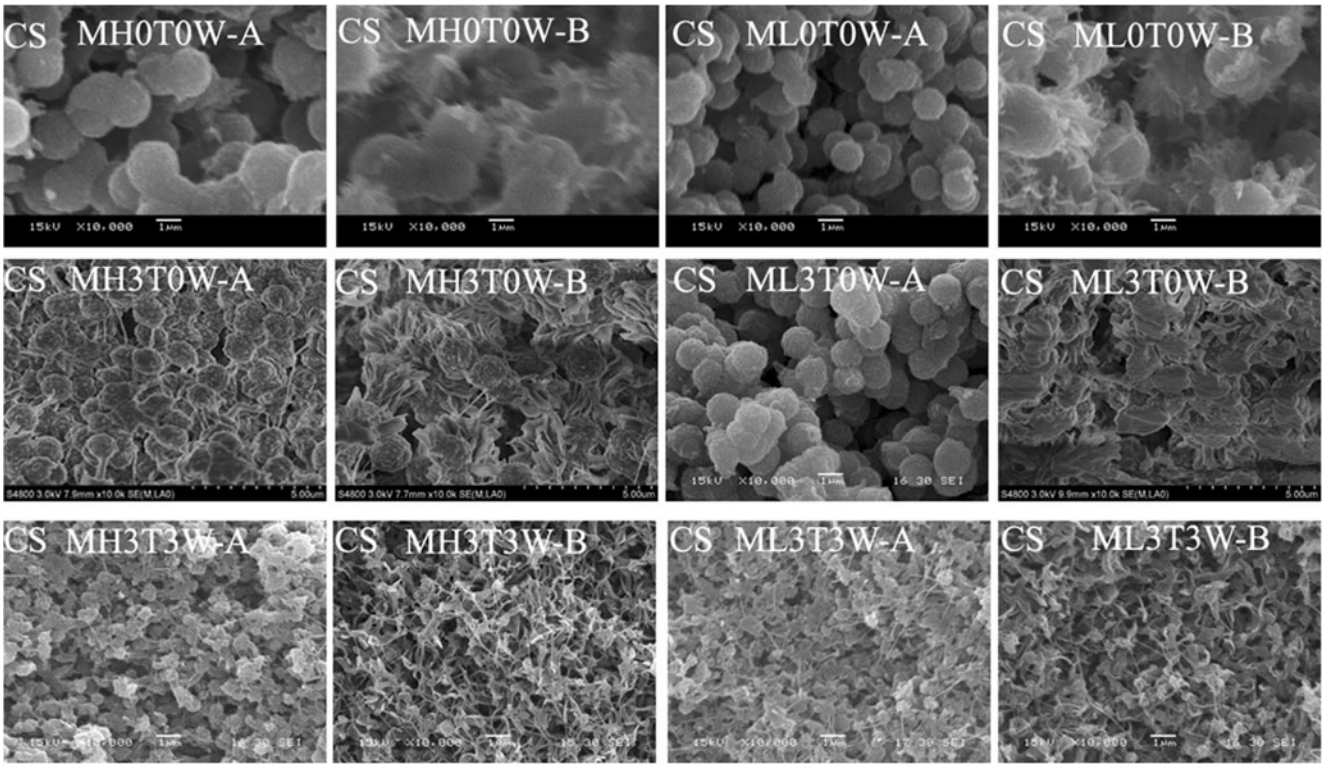

Fig. 8 SEM pictures of high magnification cross-structures (CS) of PVDF membranes prepared from two coagulants (magnification ×10,000)

Mechanical properties and crystalline structures of PVDF membranes

To investigate the relationship between membrane performance and morphology in detail, mechanical properties in terms of break strength, elongation ratio at break, and Young's modulus were measured. Figure 9 and Table 5 show that the mechanical properties improved with the addition of Tween 80. Furthermore, the membranes display excellent ductile behavior as indicated by the significantly enhanced break strength, larger elongation at break, and greatly increased Young's modulus when water is further added. These mechanical properties were further enhanced with increasing concentration of water. The order of mechanical properties of various membranes prepared with the same composition of casting solution is (MH-A) > (ML-A) > (MH-B) > (ML-B). It is noteworthy that loose-packed agglomerates of globules throughout the whole thickness of M(H)L0T0W-A(B) lad to poor mechanical properties. Therefore, dense-packed nanograins of M(H)L3T0W-A(B) explain the improved mechanical properties. Besides, the

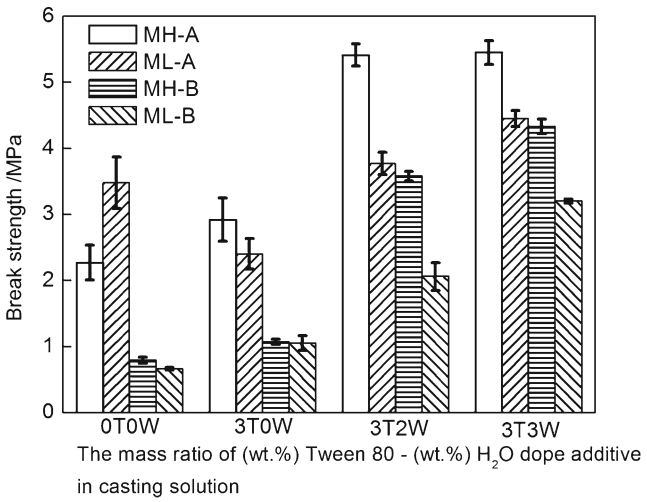

Fig. 9 Break strengths of PVDF membranes prepared under various conditions

Table 5 Elongation ratios at break and Young's modulus of membranes prepared under various conditions

Membrane	Elongation ratio at break (%)		Young's modulus (MPa)	
	A	B	A	B
MH0T0W	6.8±2.1	35.8±3.3	79.7±8.1	14.7±0.5
MH3T0W	15.0±4.2	73.0±6.8	133±4.0	19.8±3.9
MH3T2W	177±9.9	143±6.7	180±8.9	97.1±7.8
MH3T3W	272±2.2	164±6.2	194±9.3	128±8.3
ML0T0W	5.7±1.2	23.9±3.2	55.9±7.5	14.5±3.1
ML3T0W	12.6±5.6	64.5±3.8	99.8±3.6	17.7±1.9
ML3T2W	133±12.1	80.0±3.9	150±13.5	86.3±8.4
ML3T3W	248±9.0	99.1±10.0	171.3±5.4	127±5.1

A coagulant composition, water/ethanol=50:50; *B* coagulant composition, water/ethanol=0:100

porous foliage type of top surface and the slim fibril or lath bicontinuous structures of M(H)L3T3W-B bulk contribute to the limited improvement of mechanical properties. In addition, the superior mechanical properties of MH3T3W-A are attributed to dense-packed lotus-shape-type nanograins and those string- or stripe-type fine structures.

Generally, polymer crystallinity is an important factor in determining the mechanical properties as well as the impact resistance of the membranes. There are primarily four kinds of PVDF crystal structures: α, β, γ, and δ (or named II, I, III, and IV), wherein α type and β type are the main crystal structures of PVDF. The XRD data in Fig. 10 and Table 6 were used to further elucidate the crystal structure alternation of membranes caused by Tween 80/H_2O dopants, casting solution temperatures, and coagulant compositions. Figure 10 shows the XRD patters of the final membranes. Obviously, the diffraction peaks at 18.4–26.6° for membranes prepared from ethanol coagulant are much sharper than those prepared from water/ethanol, and more identifiable peaks could be found. Moreover, peaks at 2θ=18.4° and 26.6° are the characteristic of α phase. The distinct wide unresolved hybridized peak of the simultaneous presence of α and β (largely in β-phase form) clearly produces some overlap around 2θ=20°. Table 6 shows that the dominant crystalline phase of the resultant membranes is typical α and β crystal, and its degree of crystallinity increases by changing the parameters of the preparation process. It is believed that when liquid–liquid demixing takes place before crystallization, α phase is observed; whereas β phase forms when nucleation of polymer crystallites occurs within the membrane solution prior to liquid–liquid demixing [29]. Both liquid–liquid demixing and crystallization can lead to the formation of typical α and β crystal structures. The progressive crystallinity of α and β crystal type is consistent with the extent of liquid–liquid and solid–liquid demixing with variation of dopant contents, casting solution temperatures, and coagulant compositions. On the one hand, the accelerated demixing process caused by the addition of dopants and a high temperature of the casting

Table 6 XRD data of PVDF membranes prepared under various conditions [27, 29]

Membrane	2θ (θ)	*d* value	Assignment	Crystallinity (%)
MH0T0W-A	20.34	4.36	α and β	80.6
MH3T0W-A	20.26	4.38	α and β	70.9
MH3T3W-A	20.34	4.36	α and β	84
ML0T0W-A	20.16	4.40	α and β	81.8
ML3T0W-A	20.12	4.32	α and β	82.4
ML3T3W-A	18.48	4.80	α	2.1
	20.08	4.42	α and β	83.2
MH0T0W-B	18.39	4.80	α	12.1
	20.11	4.41	α and β	58.3
MH3T0W-B	18.50	4.79	α	12.9
	20.06	4.42	α and β	46.9
MH3T3W-B	18.44	4.81	α	13.5
	20.04	4.43	α and β	59.1
ML0T0W-B	18.42	4.81	α	8.2
	20.06	4.42	α and β	53.4
ML3T0W-B	18.42	4.81	α	11.5
	20.1	4.41	α and β	49.5
ML3T3W-B	18.58	4.77	α	

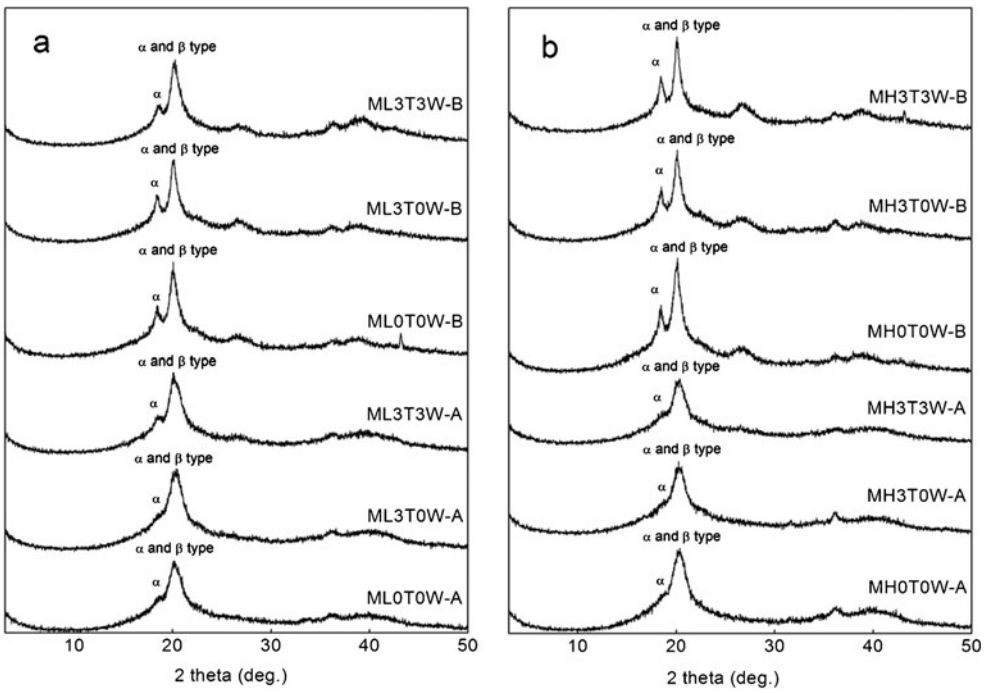

Fig. 10 XRD analysis of PVDF membranes prepared with different casting solutions (**a** 60 °C, **b** RT) in various coagulants

solution led to increasing crystallinity of α and β crystal type. On the other hand, the progressive α and β crystal type corresponds to excellent mechanical properties of the resultant membranes. The bicontinuous fine structures of string or stripe type and the maximum crystallinity of α and β type in MH3T3W-A guaranteed its superior mechanical properties.

Conclusions

High-performance PVDF membranes with interconnected bicontinuous structures were successfully prepared from water/ethanol (50:50, mass ratio) and ethanol coagulants with both 60 °C and ambient temperature casting solution, adopting Tween 80/H_2O mixtures as dopant. The influences of variations in contents of dopants, casting solution temperatures, and coagulant compositions on the phase inversion process and membrane performances in terms of configurations, hydrophilicity, filtration properties, mechanical properties, and crystallinity were investigated. The results showed that the contents of dopants, various temperatures of casting solution, and different compositions of coagulant changed the extent of liquid–liquid and solid–liquid demixing of the casting solutions. The presence of dopants in the casting solution increased the viscosity, resulting in decreasing surface tension and accelerating the precipitation rate. During the demixing process, water diffusing out from Tween 80 reverse micelles broke the equilibrium between the interaction between the polar heads of the surfactant and water and the interconnection between PVDF and hydrophobic chains of the surfactant. This confined diffusion of water favored the surface segregation of the polar head groups of Tween 80, which contributed to the improvement of the hydrophilicity of the resultant membranes. Besides, the high temperature of the casting solution explained the enhanced diffusion rate of liquid–liquid demixing on crystallization. The high temperature of the casting solution in water/ethanol coagulant facilitated the demixing process of PVDF/DMAc/Tween 80/water systems. On the one hand, the less delayed demixing process favored the formation of bicontinuous fine structure in the form of strings or stripes. On the other hand, the shorter demixing process confined the surface segregation of Tween 80, leading to limited improvement in the hydrophilicity of the resultant membranes. Furthermore, the shorter demixing process resulted in both liquid–liquid demixing and crystallization, which led to progressive crystallinity of α and β crystal type and guaranteed superior mechanical properties of MH3T3W-A. This revealed that the crystallization of PVDF/DMAc/Tween 80/water systems in ethanol coagulant occurred prior to liquid–liquid demixing. This explained the formation of porous foliage-type top structures, the high flux, and the significant hydrophilicity improvement of PVDF membranes.

Acknowledgment The authors are grateful for financial support from the Key Technology R&D Program of Shanghai Committee of Science and Technology in China (11DZ1205201) and the Key Program of Science and Technology of Guangdong Province in China (2011A080403004).

References

1. Strathmann H (2001) Membrane separation processes: current relevance and future opportunities. AICHE J 47:1077–1087
2. Liu F, Hashim NA, Liu Y, Abed MRM, Li K (2011) Progress in the production and modification of PVDF membranes. J Membr Sci 375:1–27
3. Don T-M, Hsu Y-C, Tai H-Y, Fu E, Cheng L-P (2012) Preparation of bi-continuous macroporous polyamide copolymer membranes for cell culture. J Membr Sci 415–416:784–792
4. Liu F, Tao M-m, Xue L-x (2012) PVDF membranes with interconnected pores prepared via a Nat-ips process. Desalination 298:99–105
5. Khayet M, Matsuura T (2001) Preparation and characterization of polyvinylidene fluoride membranes for membrane distillation. Ind Eng Chem Res 40:5710–5718
6. Wang X, Zhang L, Sun D, An Q, Chen H (2008) Formation mechanism and crystallization of poly(vinylidene fluoride) membrane via immersion precipitation method. Desalination 000:1–9
7. Yeow ML, Liu YT, Li K (2003) Isothermal phase diagrams and phase-inversion behavior of poly(vinylidene fluoride)/solvents/additives/water systems. J Appl Polym Sci 90:2150–2155
8. Shi L, Wang R, Cao Y (2009) Effect of the rheology of poly (vinylidene fluoride-co-hexafluropropylene) (PVDF–HFP) dope solutions on the formation of microporous hollow fibers used as membrane contactors. J Membr Sci 344:112–122
9. Hester JF, Mayes AM (2002) Design and performance of foul-resistant poly(vinylidene fluoride) membranes prepared in a single-step by surface segregation. J Membr Sci 202:119–135
10. Curcio E, Fontananova E, Profio GD, Drioli E (2006) Influence of the structural properties of poly(vinylidene fluoride) membranes on the heterogeneous nucleation rate of protein crystals. J Phys Chem B 110:12438–12445
11. Wang DL, Li K, Teo WK (2000) Porous PVDF asymmetric hollow fiber membranes prepared with the use of small molecular additives. J Membr Sci 178:13–23
12. Yuliwati E, Ismail AF (2011) Effect of additives concentration on the surface properties and performance of PVDF ultrafiltration membranes for refinery produced wastewater treatment. Desalination 273:226–234
13. Sukitpaneenit P, Chung T-S (2009) Molecular elucidation of morphology and mechanical properties of PVDF hollow fiber membranes from aspects of phase inversion, crystallization and rheology. J Membr Sci 340:192–205
14. Younga TH, Cheng LP, Linb D, Faneb L, Chuanga WY (1999) Mechanisms of PVDF membrane formation by immersion-precipitation in soft (1-octanol) and harsh (water) nonsolvents. Polymer 40:5315–5323
15. Deshmukh SP, Li K (1998) Effect of ethanol composition in water coagulation bath on morphology of PVDF hollow fibre membranes. J Membr Sci 150:75–85
16. Zhang PY, Yang H, Xu ZL (2012) Preparation of polyvinylidene fluoride (PVDF) membranes via nonsolvent induced phase separation process using a Tween 80 and H_2O mixture as an additive. Ind Eng Chem Res 51:4388–4396
17. Hester JF, Banerjee P, Mayes AM (1999) Preparation of protein-resistant surfaces on poly(vinylidene fluoride) membranes via surface segregation. Macromolecules 32:1643–1650

18. Hester JF, Olugebefola SC, Mayes AM (2002) Preparation of pH-responsive polymer membranes by self-organization. J Membr Sci 208:375–388
19. Zhang PY, Wang YL, Xu ZL, Yang H (2011) Preparation of poly (vinyl butyral) hollow fiber ultrafiltration membrane via wet-spinning method using PVP as additive. Desalination 278:186–193
20. Yang Q, Xu ZK, Dai ZW, Wang J, Ulbricht M (2005) Surface modification of polypropylene microporous membranes with a novel glycopolymer. Chem Mater 17:3050–3058
21. Manful JT, Grimm CC, Gayin J, Coker RD (2008) Effect of variable parboiling on crystallinity of rice samples. Cereal Chem 85:92–95
22. Yun YB, Zhang PY, Zhu MH, Liu C, Wang LH, Chen CX, Li JD (2012) Correction to preparation and characterization of poly(phthalazinone ether sulfone) hollow fiber ultrafiltration membranes. Langmuir 28:10627−10627
23. Panu S, Chung TS (2009) Molecular elucidation of morphology and mechanical properties of PVDF hollow fiber membranes from aspects of phase inversion, crystallization and rheology. J Membr Sci 340:192–205
24. Ghosh S (2011) Comparative studies on brij reverse micelles prepared in benzene/surfactant/ethylammonium nitrate systems: effect of head group size and polarity of the hydrocarbon chain. J Colloid Interface Sci 360:672–680
25. Basílio N, Garcia-Rio L, Martín-Pastor M (2012) Calixarene-based surfactants: evidence of structural reorganization upon micellization. Langmuir 28:2404–2414
26. Amirilargani M, Saljoughi E, Mohammadi T (2010) Improvement of permeation performance of polyethersulfone (PES) ultrafiltration membranes via addition of Tween-20. J Appl Polym Sci 115:504–513
27. Yang Q, Kang XZ, Wei DZ, Li WJ, Ulbricht M (2005) Surface modification of polypropylene microporous membranes with a novel glycopolymer. Chem Mater 17:3050–3058
28. Lin DJ, Beltsios K, Chang CL, Cheng LP (2003) Fine structure and formation mechanism of particulate phase-inversion poly(vinylidene fluoride) membranes. J Polym Sci B Polym Phys 41:1578–1588
29. Buonomenna MG, Macchi P, Davoli M, Drioli E (2007) Poly (vinylidene fluoride) membranes by phase inversion: the role the casting and coagulation conditions play in their morphology, crystalline structure and properties. Eur Polym J 43:1557–1572
30. Teshima K, Sugimura H, Inoue Y, Takai O, Takano A (2003) Ultra-water-repellent poly(ethylene terephthalate) substrates. Langmuir 19:10624–10627